A Supply-Voltage Driving Scheme for Grounded Capacitive Sensor Front-Ends

Marcelo Alejandro Haberman, Enrique Mario Spinelli, and Ferran Reverter

***Abstract*— In this article, a novel supply-voltage driving (SVDR) scheme for capacitive sensor front-ends is proposed to eliminate the parasitic capacitance effects. The suggested circuit is intended for remote sensors (and, hence, connected to the circuit through a shielded cable) with one electrode grounded and of low capacitance (in the 0–10-pF range). The effects of the parasitic capacitance of the cable are avoided using the active-shielding technique, whereas those of the amplifier input through a smart driving of the reference node of the amplifier supply voltage. Thanks to these techniques, the input–output characteristic shows, without applying any adjustment and/or calibration, an offset error lower than 3 fF. The nonlinearity error (NLE) is in the order of 0.01% of the full-scale span (FSS), which corresponds to 1 fF. Different operational amplifiers (OAs) and different lengths (up to 15 m) of the interconnecting cable are experimentally tested to demonstrate the feasibility of the circuit. In comparison with similar circuits recently suggested in the literature, the proposed circuit does not require any bulky component, such as a transformer, and consequently, it is a lower-cost solution and suitable to be integrated.**

***Index Terms*— Active shielding, capacitance, capacitance measurement, capacitive sensors, front-end circuit, grounded capacitive sensor, sensor interface electronics, stray capacitance.**

I. Introduction

IN THE era of the Internet of Things and Industry 4.0, the role of sensors is increasingly relevant. Advances in the field of sensors have promoted the concept of smart sensors or sensor 4.0, offering advantages such as better performance, higher integration, and self-calibration [1]. These smart sensors can rely on different types of sensing elements (e.g., resistive, capacitive, and inductive) with different topologies (e.g., single element, differential, and bridge type). Single-element capacitive sensors, with an electrical capacitance that changes with the quantity being monitored, are quite common in the industrial, automotive, laboratory, and healthcare [2], [3] applications. These sensors are employed, for example, to monitor magnitudes such as pressure, acceleration, humidity [4], liquid level [5], distance, displacement, and flow [6].

Manuscript received 30 March 2022; revised 20 July 2022; accepted 28 August 2022. Date of publication 12 September 2022; date of current version 26 September 2022. This work was supported in part by the CONICET under Project PIP-0323, in part by La Plata National University (UNLP) under Project I254 and Project PPID/I014, and in part by the Agencia I+D+i under Project PICT 2018-03747. The Associate Editor coordinating the review process was Dr. Boby George. *(Corresponding author: Marcelo Alejandro Haberman.)*

Marcelo Alejandro Haberman and Enrique Mario Spinelli are with the Institute for Research in Electronics, Signal Processing, and Control (LEICI), La Plata National University (UNLP), CONICET, La Plata 1900, Argentina (e-mail: marcelo.haberman@ing.unlp.edu.ar).

Ferran Reverter is with the Department of Electronic Engineering, Universitat Politècnica de Catalunya (Barcelona Tech), 08860 Barcelona, Spain (e-mail: ferran.reverter@upc.edu).

Digital Object Identifier 10.1109/TIM.2022.3205648

Capacitive sensors offer advantages in terms of cost, power consumption, and robustness, but the design of the ensuing read-out circuit can be quite complex, especially when the sensor has a low capacitance (i.e., units of pF or less) and is remote (i.e., it is connected to the circuit via a shielded cable). Note that, in some applications, the parasitic capacitance of the cable can be up to three orders of magnitude higher than the sensor capacitance.

Within the category of capacitive sensors, two subgroups can be distinguished [7]: floating and grounded. In the former subgroup, the two sensor electrodes are not connected by default to any potential, whereas in the latter, one of the two electrodes is always connected to the ground. The design of the read-out circuit is easier, and also more studied in the literature, for the floating type, particularly when the sensor is remote. In such a case, connecting the cable shield to the ground (which is known as passive shielding) is not a major problem, but it is for the grounded type since the cable parasitic capacitance is in parallel with the sensor capacitance. This makes the floating type more attractive than the grounded counterpart. However, due to safety reasons and/or limitations imposed by the application, grounding one of the electrodes is unavoidable, and special read-out circuits for grounded capacitive sensors must be used. That happens, for example, in the level measurement of a conductive liquid in a grounded metallic container [8], where the grounded liquid behaves as one of the plates of a capacitance proportional to the liquid level, and an isolated metal rod is the second plate, that is connected to the read-out circuit. A similar situation occurs in the distance/proximity measurement to grounded metallic objects [9] or to detect the proximity of subjects [10], which are considered to be grounded through a 100–200-pF coupling capacitance [11], which is two or three orders of magnitude higher than the sensor capacitance. Another situation where one of the plates of the capacitive sensor is forced to ground is for linear/angular displacement measurement of a grounded shaft [12].

The read-out circuits proposed in the literature for grounded capacitive sensors employ two different types of excitation: square and sinusoidal. The former excitation is more easily generated, but the latter has the advantage that an appropriate selection of the excitation frequency can make the sensor parasitic components negligible. As for the square excitation, it has been proposed the direct connection of the sensor to a microcontroller that measures the charging/discharging time of an RC circuit [13]. This is a simple solution, but not applicable to remote grounded capacitive sensors since it has no mechanism to compensate for the parasitic capacitance of the cable. In order to cope with this limitation, relaxation oscillators complemented with the active-shielding technique have been suggested [8], [14], [15]. When the active shielding is applied, the shield of the interconnecting cable is not connected to the ground, but it is driven at the same potential as that of the inner conductor, for example, via a voltage follower. Although such oscillators have good performance even for long interconnecting cables, these require continuous auto-calibration that involves the measurement of the offset capacitance caused by the devices and tracks of the printed circuit board (PCB). With square excitation, the semiconductor market offers chips specifically designed for grounded capacitive sensors, such as the AD7747 from Analog Devices. However, the measurement error of these integrated solutions clearly deteriorates for long interconnecting cables. On the other hand, for sinusoidal excitation, different types of ac bridges based on operational amplifiers (OAs) have been proposed in the literature [9], [12], [16]. To avoid the coupling of external interference and to minimize the parasitic capacitances between the environment and the sensor or the interconnecting cable, some of these proposals are complemented with passive shielding [9] (i.e., the shield capacitance is in parallel with the sensor) and others with active shielding [12] that removes the offset effect of the shield capacitance but not that of the input capacitance of the circuit. In both cases, there is a remaining offset capacitance produced by the shield and/or the circuit. With sinusoidal excitation, a novel transformer-based ac bridge with a very low offset capacitance (to be precise, less than 2 fF for a 12-m interconnecting cable) was presented in [17]. Its main limitation, however, is the volume and cost of the required transformer, and the fact that this is not suitable to be integrated.

In the context explained before, a novel front-end circuit for grounded capacitive sensors is introduced and evaluated, both theoretically and experimentally, in this article. The proposed circuit applies sinusoidal excitation and active shielding. Unlike most of the circuits suggested in the literature, excluding [17], the novel circuit does not require either a measurement of the offset capacitance or a component adjustment to compensate for the effects of the offset capacitance, thus simplifying the calibration process. In addition, with respect to the circuit recently proposed in [17], the novel circuit does not rely on a transformer, thus resulting in a low-cost, compact design solution, suitable to be integrated. As explained in more detail in the following sections, the novel circuit is based on a smart driving of the reference node of the OA supply voltage. By means of this idea, the resulting output signal becomes independent of the OA input capacitance and also of the parasitic capacitance of the interconnecting cable.

The article is organized as follows. Section II describes the operating principle of the proposed circuit. In Section III, the behavior of the circuit against nonidealities is theoretically analyzed. Sections IV and V explain the materials and methods and the corresponding experimental results, respectively. Finally, Section VI draws the main conclusions.

II. Operating Principle

The auto-balancing bridge (ABB), also known as an ac bridge with current detection, is a usual and effective method to measure floating capacitors [18], [19]. Fig. 1(a) shows a typical scheme applying passive shielding where C_X is the capacitance of the remote sensor, v_R is a sinusoidal reference signal with rms value V_R and frequency f_R, C_{IN} is the OA input capacitance, and C_{SH} represents the stray capacitance of the shielded cable and PCB tracks. Assuming an ideal OA, the voltages across C_{SH} and C_{IN} are null because of the virtual ground it imposes. Then, these capacitances do not affect the

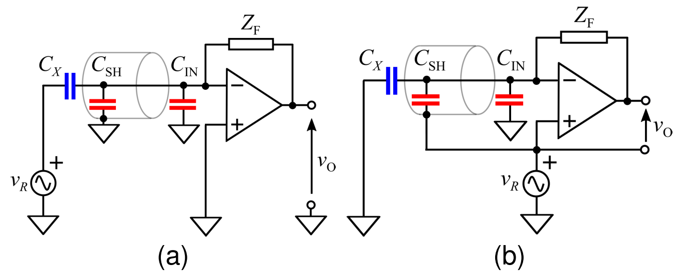

Fig. 1. (a) Auto-balancing ac bridge for floating capacitances and (b) version for grounded capacitances that drives the shield to avoid C_{SH} effect.

output voltage v_O, which is a sinusoidal signal whose rms value V_O is given by (1). This value is proportional to C_X and allows to estimate it

$$V_O = V_R 2\pi f_R |Z_F| C_X. \tag{1}$$

The ABB in Fig. 1(a) can be adapted to grounded capacitances by moving the generator v_R to the noninverting input of the OA and defining a differential output v_O, as shown in Fig. 1(b) [20], [21], [22]. The effect of the shield capacitance C_{SH} can be avoided by applying the active-shielding technique, that is, by driving it at the potential v_R. In this way, no voltage difference appears across C_{SH}, no current flows through it, and does not contribute to V_O. Nevertheless, this technique cannot be applied directly to C_{IN}, because one of its terminals is not available and, hence, the effect of C_{IN} remains and (1) becomes

$$V_O = V_R 2\pi f_R |Z_F| (C_X + C_{\mathrm{IN}}). \tag{2}$$

The circuit in Fig. 1(b), with some variations, has been used to measure the liquid level in metallic tanks [20] and to estimate the coupling capacitance in noncontact ac voltage measurements [21], [22], but forces to adjust a compensation current or to include a digital calibration procedure to disaffect C_{IN}. The method works for C_X as low as a few pF, but its accuracy is limited by C_{IN} variations from the adjustment/calibration time to the measurement time. Any drift on C_{IN} directly affects the measurement of C_X.

In an OA with a split supply voltage, C_{IN} is not actually connected to the ground since the OA does not have a ground terminal. This parasitic capacitance is the consequence of the capacitances C_{IN}^-, C_{IN}^+ present from the OA input node to the power supply rails [23], [24]. As shown in Fig. 2(a), for ac signals, these capacitances are connected to the ground through the positive and negative dc sources V_P and V_N, thus resulting in an effective input capacitance $C_{\mathrm{IN}} = C_{\mathrm{IN}}^- + C_{\mathrm{IN}}^+$ and (2) can be rewritten as

$$V_O = V_R 2\pi f_R |Z_F| \left(C_X + C_{\mathrm{IN}}^- + C_{\mathrm{IN}}^+\right). \tag{3}$$

Taking into account the previous issue related to C_{IN}, here we propose the novel circuit shown in Fig. 2(b) for the measurement of grounded capacitances. This relies on removing the ground at the middle point between V_P and V_N and connecting it to v_R. This ABB with Supply-Voltage DRiving (SVDR) avoids the effects of C_{IN}^-, C_{IN}^+ because their terminals equally vary with v_R. No potential variation appears across them, no current flows through them, and, therefore, their effects vanish. In this condition, the circuit is insensitive to parasitic capacitances and also to their time drifts, and the

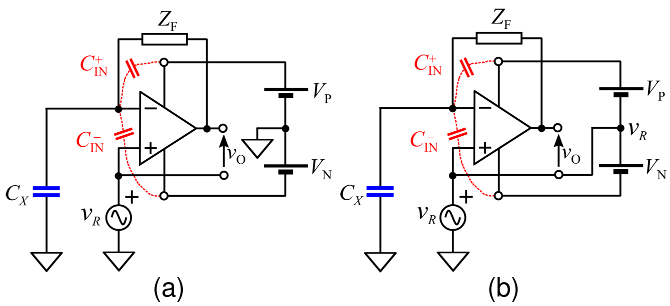

Fig. 2. (a) Auto-balancing ac bridge for grounded capacitances including input capacitances and dc power supply sources. (b) Proposed circuit that drives both power-supply rails by v_R.

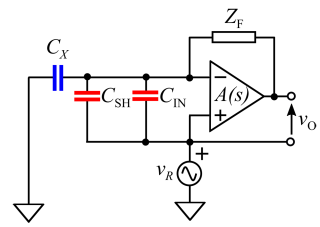

Fig. 3. AC model used to compute circuit's transfer function. It takes into account the finite open-loop gain of OA and the parasitic capacitances.

output V_O verifies (1). It works as well as the well-known ABB but deals with grounded capacitances. The fact of being independent of C_{IN} also allows us to select an OA without any limitation on this parameter. For example, very low noise OAs, which offer very high input capacitances, can be employed without any side effects.

The proposed solution based on SVDR is similar to power-supply bootstrapping (PSB) schemes [23], [24], [25] used also to cancel the effects of the input capacitance in voltage buffers. However, the main difference is that the PSB solution involves the feedback of the amplifier output to the power supply pins, while the proposed SVDR is feedforward based, avoiding the stability issues that the PSB has [25].

The circuit in Fig. 2(b) provides a sinusoidal output v_O, whose amplitude is proportional to C_X, but its phase delay with respect to v_R depends on the feedback impedance Z_F. If it is capacitive, v_O and v_R are in phase, but if Z_F is resistive, v_O and v_R are in quadrature. The former is known as a charge amplifier (CA), whereas the latter is a trans-impedance amplifier (TIA). In the following, and without loss of generality over the proposed SVDR, we assume the last case, where $Z_F = R_F$ and (1) becomes

$$V_{OQ} = V_R 2\pi f_R R_F C_X \tag{4}$$

where V_{OQ} is the rms value of the output component in quadrature with the sinusoidal reference v_R. The capacitance C_X can be estimated from V_{OQ} as

$$C_X = V_{OQ}/(V_R 2\pi f_R R_F) = V_{OQ} K \tag{5}$$

where $K = (V_R 2\pi f_R R_F)^{-1}$ is the factor that linearly relates the output voltage and C_X.

III. Theoretical Analysis of Circuit Nonidealities

The solution depicted in Fig. 2(b) relies on the null voltage difference between the OA's inputs that the negative feedback forces, which is valid only for an ideal infinite open-loop gain of the OA. To determine a usable operating frequency range and predict the error on the measurement of C_X, a more realistic model is applied herein, considering a finite OA open-loop gain, $A(s)$, and the parasitic capacitances in the feedback path. This ac signal model is depicted in Fig. 3, where the dc power supplies behave as short circuits, thus C_{IN}^- and C_{IN}^+ are in parallel, resulting in the equivalent input capacitance C_{IN}. Also, the capacitance C_{SH} is included, regarding the shield capacitance of the interconnecting cable (50–100 pF/m).

The analysis of the circuit in Fig. 3 shows that the transfer function from v_R to v_O is

$$\begin{aligned} T(s) &= \frac{V_O(s)}{V_R(s)} \\ &= sC_X Z_F \left[\frac{A(s)}{A(s) + 1 + s(C_X + C_{SH} + C_{IN})Z_F}\right] \end{aligned} \tag{6}$$

which, at ideal conditions with $A(s) = \infty$, is simplified to $T_I(s) = sC_X Z_F$ that agrees with (4).

The OA open loop gain, $A(s)$, includes its dc finite gain A_0 and a single pole at $s = -\omega_{GBP}/A_0$, where ω_{GBP} is the gain-bandwidth product of the OA

$$A(s) = \frac{A_0}{1 + sA_0/\omega_{GBP}}. \tag{7}$$

For frequencies greater than 1 kHz, (7) can be further simplified to an integrative transfer function [26]

$$A(s) = \frac{\omega_{GBP}}{s}. \tag{8}$$

By replacing (8) in (6), and considering $Z_F = R_F$, the following expression for $T(s)$ is obtained:

$$\begin{aligned} T(s) &= sC_X R_F \left[\frac{1}{1 + \frac{s}{\omega_{GBP}} + s^2 \frac{(C_X + C_{SH} + C_{IN})R_F}{\omega_{GBP}}}\right] \\ &= T_I(s) T_{NI}(s) \end{aligned} \tag{9}$$

which is the ideal response affected by the second-order low-pass transfer function $T_{NI}(s) = [1+(s/\omega_{GBP})+s^2((C_X+C_{SH}+C_{IN})R_F/\omega_{GBP})]^{-1}$ that accounts for the finite OA open-loop gain and the parasitic capacitances involved.

The natural frequency of $T_{NI}(s)$ is $\omega_n = (\omega_{GBP}/[R_F(C_X + C_{IN} + C_{SH})])^{1/2}$ and its computation is useful to choose an operating frequency $\omega_R = 2\pi f_R$ lower enough to make the effect of $T_{NI}(s)$ on the measurement of C_X negligible. V_{OQ} is affected by such nonidealities in the following way:

$$\begin{aligned} V_{OQ} &= V_R \cdot \mathrm{Imag}(T(j\omega_R)) \\ &\approx V_R \omega_R R_F C_X \left(1 + \left(\frac{\omega_R}{\omega_n}\right)^2\right) \end{aligned} \tag{10}$$

where to reach the approximated expression (10), it is assumed that $\omega_{GBP} \gg \omega_R$ and that $\omega_{GBP} \gg {\omega_R}^2 C_{SH}(C_X + C_{IN} + C_{SH})$. Comparing (4) and (10), the nonidealities of the circuit generate a gain error in the input–output characteristic. In addition, the longer the cable, the lower ω_n and the higher the gain error. This gain error can be approximated to

$$e_{NI} \approx (\omega_R/\omega_n)^2. \tag{11}$$

For example, considering a TIA transimpedance factor of $R_F = 4.7$ MΩ, a 1-m interconnecting cable ($C_{SH} \approx 60$ pF),

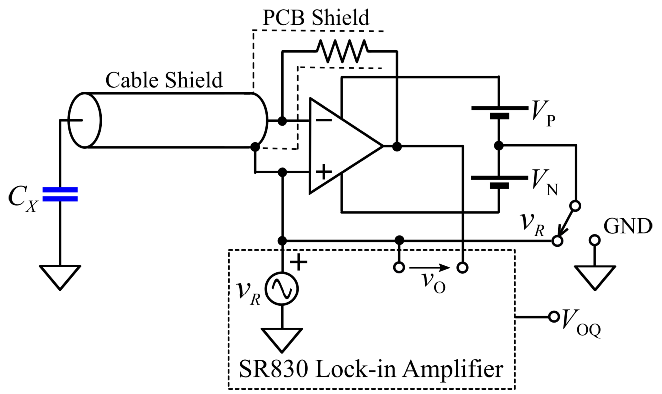

Fig. 4. Simplified schematic of the experimental setup used to validate the proposed front-end circuit with SVDR. When the middle point of V_P and V_N is connected to the ground, the front-end circuit is in the ABB mode, while connecting it to v_R, the circuit is in the SVDR mode.

a sensor capacitance of $C_X = 10$ pF, and a TLC2202 OA ($\omega_{\text{GBP}} = 2\pi 1.9$ MHz and $C_{\text{IN}} \approx 22$ pF) will lead to $\omega_n \approx 2\pi 26$ kHz. If an OPA320 OA ($\omega_{\text{GBP}} = 2\pi 20$ MHz and $C_{\text{IN}} \approx 1$ pF) is used instead, the natural frequency will be $\omega_n \approx 2\pi 98$ kHz. Thus, for an operating frequency $f_R = 2$ kHz, the gain error due to circuit nonidealities, e_{NI}, is expected to be 0.57% and 0.04% for each OA, respectively. However, the same circuit applied to measuring a remote sensor at 15 m of distance ($C_{\text{SH}} \approx 900$ pF) leads to $\omega_n \approx 2\pi 8$ kHz (TLC2202) and $\omega_n \approx 2\pi 27$ kHz (OPA320) with expected gain errors of 5.8% and 0.54%. Note that these expected errors were computed using (11) and multiplied by a factor of 100 to express them as a percentage.

It is worth to note, besides the gain error introduced by the circuit nonidealities, that the offset error of the front-end circuit is theoretically zero (which is the main goal of the proposed solution), even for remote measurements with very long interconnecting cables. Therefore, the error that the interconnecting cables introduce can be addressed by a simple one-point calibration (OPC) of the constant K used in (5).

IV. Materials and Method

An experimental setup and a circuit prototype were implemented to validate the effectiveness of the proposed circuit to reject C_{IN} and C_{SH} effects. The general scheme is shown in Fig. 4. The OA works as a TIA with a nominal transimpedance factor of $R_F = 4.7$ MΩ. A shield of the OA inverting input was implemented in the PCB and connected to v_R together with the shield of the coaxial cable. The sinusoidal reference v_R was provided by a lock-in amplifier (Stanford Research 830) which also measured the quadrature component V_{OQ}. Alkaline AA batteries were used for the dc sources V_P and V_N composing the split supply voltage. A switch in the common node between V_P and V_N allowed us to connect it to the ground or v_R: the first case corresponds to the ABB circuit and the last to the technique herein proposed.

Two TIAs were built using different OAs: the TLC2202 and the OPA320, both from Texas Instruments, with a gain-bandwidth product of 1.9 and 20 MHz, respectively. The OA election was addressed to test the proposed technique for devices with very different input capacitance. The input capacitance of the TLC2202 is not listed on its datasheet, but measurements of this parameter in the range of 20–30 pF were reported [27], [28], whereas the OPA320 presents a significantly lower C_{IN} of just a few pF. The TLC2202 was powered by $V_P = V_N = 3$ V (four AA batteries) and the OPA320 with $V_P = V_N = 1.5$ V (two AA batteries).

TABLE I
Experimental Results for 1-m Cable

LCR meter [pF]	OPA320 ABB [pF]	OPA320 SVDR [pF]	TLC2202 ABB [pF]	TLC2202 SVDR [pF]
0	1.0956	0.0022	21.7788	0.0023
1.2332 (±0.7 fF)	2.3347	1.2411	22.9945	1.2477
3.9816 (±0.2 fF)	5.0963	4.0060	25.7899	4.0280
5.7300 (±0.6 fF)	6.8521	5.7617	27.5609	5.7939
8.3610 (±0.7 fF)	9.4951	8.4030	30.2225	8.4521
10.1374 (±0.8 fF)	11.2763	10.1876	32.0257	10.2486

A set of ceramic capacitors ranging from 0 to 10 pF (to be precise, with a nominal value of 0, 1.2, 3.9, 5.6, 8.2, and 10 pF) emulated the sensor capacitance C_X. These were first measured with an LCR meter (LCR-819 from GW-Instek) at a frequency of 2 kHz, as floating capacitances placed inside a shield box as in [17]. Then, these were measured again grounding one of their terminals by the proposed circuit (SVDR) and with the conventional ABB method. All these measurements were performed for a sinusoidal reference v_R of 100 mV_{rms} and 2 kHz, which is lower than the values of ω_n theoretically reported in Section III.

The capacitors emulating C_X were connected via a V45466-D13-C15 coaxial cable of different lengths to the circuit shown in Fig. 4. The default length was 1 m with $C_{\text{SH}} \approx 60$ pF, but additional tests were also carried out at longer interconnecting cables (5, 10, and 15 m) to observe the effects of the parasitic components on the input–output characteristic.

The robustness of the proposed circuit in front of time drifts of C_{IN} was also evaluated experimentally by taking samples every 10 min on three different days. The experimental setup of Fig. 4 was employed to measure a 1.2-pF capacitor in both modes (ABB and SVDR), using the TLC2202 and a 1-m interconnecting cable. For the SVDR mode, C_X was computed by (5), and for the ABB mode by

$$C_X^{\text{ABB}} = V_{\text{OQ}} K - C_{\text{IN}} \tag{12}$$

where C_{IN} was measured only once at the beginning of the experiment the first day, by emptying the shield box, leading to $C_{\text{IN}} = 21.978$ pF according to (5).

V. Experimental Results

A. Input–Output Characteristic for a 1-m Cable

Table I summarizes the experimental results when using a 1-m interconnecting cable. The first column contains the measurements of the capacitances with the LCR meter; the mean and standard deviation of seven consecutive measurements. The second to fifth columns show, for the two OAs and the two modes under test, the value of C_X resulting from the application of (5) to the measured values of V_{OQ}, with a proportional constant $K = (V_R 2\pi f_R R_F)^{-1} = 0.169314$ pF/mV computed from nominal values.

Fig. 5 shows the capacitances measured by the front-end circuit built with the OPA320 for the two measurement modes (ABB and SVDR, the second and third columns of Table I, respectively) plotted against the reference measurement done with the LCR meter (the first column of Table I). The difference between ABB and SVDR measurements for each test

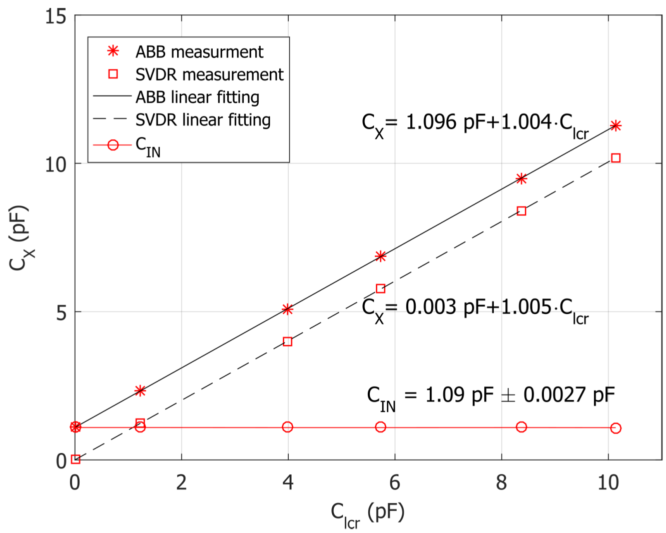

Fig. 5. Measurements of grounded capacitors made with the front-end circuit based on OPA320, for ABB and SVDR modes. The difference between the two measurements modes is plotted as C_{IN}.

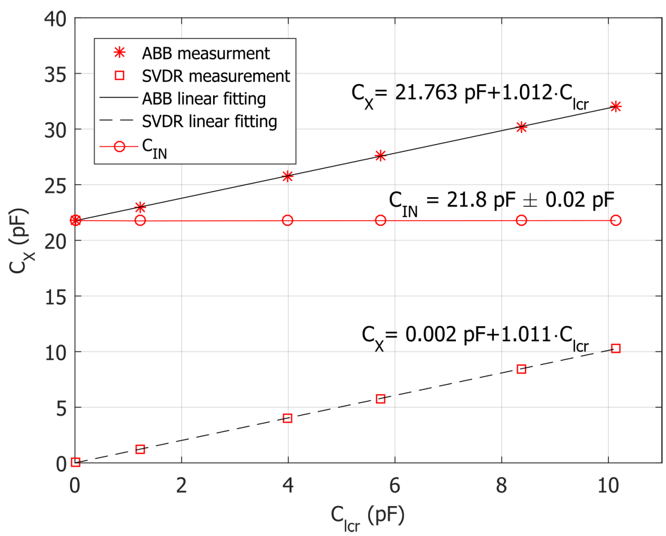

Fig. 6. Measurements of grounded capacitors made with the front-end circuit based on TLC2202 for ABB and SVDR modes. The difference between the two measurements modes is plotted as C_{IN}.

capacitor that is explained by the input capacitance C_{IN} is also plotted. The linear fittings by the least-square method, used later in the linearity analysis, are also shown for both measurement modes. Similarly, Fig. 6 depicts the information about the measurements carried out with the front-end circuit based on the TLC2202 (the fourth and fifth columns of Table I). Here, the difference between the two modes becomes higher since the input capacitance of the TLC2202 is higher, to be precise: 1.09 pF in Fig. 5 and 21.8 pF in Fig. 6. According to Figs. 5 and 6, the measurement of grounded capacitances performed with the SVDR technique is immune to the value of C_{IN}, without any manual adjustment or calibration.

B. Error Analysis With and Without Calibration

Fig. 7 shows the absolute error (in pF) of the grounded capacitance measurements made with both OAs on the SVDR mode with respect to the reference measurements made with the LCR meter. Accordingly, the higher the value of the

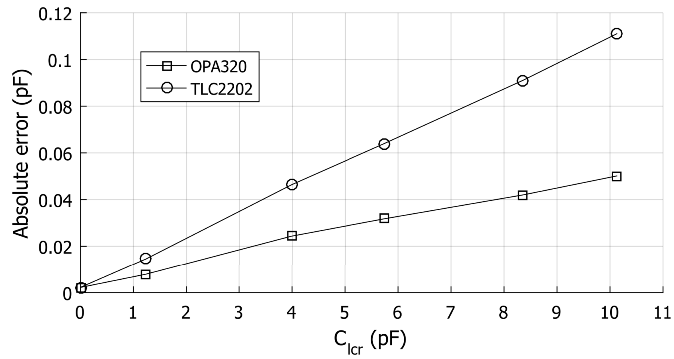

Fig. 7. Absolute error between capacitance measured with the proposed method for grounded capacitors and the floating measurement done with the LCR meter.

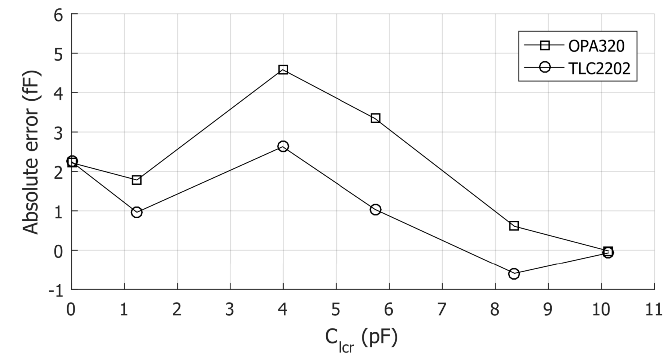

Fig. 8. Absolute errors recomputed after applying the OPC.

capacitance to be measured, the higher the error, which means that the system is subjected to a gain error. This is caused by the nonidealities analyzed in Section III and also by the tolerance of the TIA resistor, given that the measured capacitances listed in Table I were computed by (5) assuming the nominal values of R_F, V_R, and f_R in K. For the OPA320, the maximum error was 50 fF [which corresponds to 0.5% of the full-scale span (FSS)], whereas, for the TLC2202, it was 120 fF (1.2 %FSS).

Given the linear relationship and the zero offset of the proposed circuit inferred from (4), (5), and even (10), the gain error represented before in Fig. 7 can be easily reduced by means of an OPC. It is proposed to use the output obtained for the highest capacitance under test (see Table I) to correct the proportionality constant for both OAs, that is, $K_{\mathrm{OPA}} = K \cdot 10.1374/10.1876$ and $K_{\mathrm{TLC}} = K \cdot 10.1374/10.2486$. Assuming such new values of the proportionality constant, the resulting absolute errors are represented in Fig. 8. In such conditions, for the OPA320, the maximum error is 4.5 fF (which corresponds to 0.045 %FSS), whereas, for the TLC2202, it is 2.5 fF (0.025 %FSS). The reduction of error, in comparison to Fig. 7, is higher than 10 for the OPA320 and almost 50 for the TLC2202.

C. Nonlinearity Error

As explained in Section V-B, the linearity of the system is needed to easily correct the gain error by a simple OPC, and it is usually assessed by the nonlinearity error (NLE) [8], [17], [19]. It was computed as the difference between each

TABLE II
EXPERIMENTAL RESULTS FOR DIFFERENT CABLE'S LENGTH

	OPA320			TLC2202		
LCR meter [pF]	**5 m [pF]**	**10 m [pF]**	**15 m [pF]**	**5 m [pF]**	**10 m [pF]**	**15 m [pF]**
0	0.0023	0.0023	0.0023	0.0024	0.0025	0.0026
1.2346	1.2397	1.2412	1.2432	1.2559	1.2794	1.3043
5.7355	5.7451	5.7536	5.7637	5.8215	5.9303	6.0459
10.117	10.1307	10.1475	10.1627	10.2697	10.4606	10.6649
Fitting offset [fF]	3.0	2.7	3.0	2.4	2.7	2.7
Fitting gain	1.0011	1.0027	1.0042	1.0148	1.0337	1.0538
Gain error [%FSS]	0.11 %	0.27 %	0.42 %	1.48 %	3.37 %	5.38 %
Expected gain error from (11) **[%FSS]**	0.18 %	0.36 %	0.54 %	2.06 %	3.93 %	5.79 %
MNLE [%FSS]	0.008 %	0.006 %	0.007 %	0.013 %	0.009 %	0.011 %

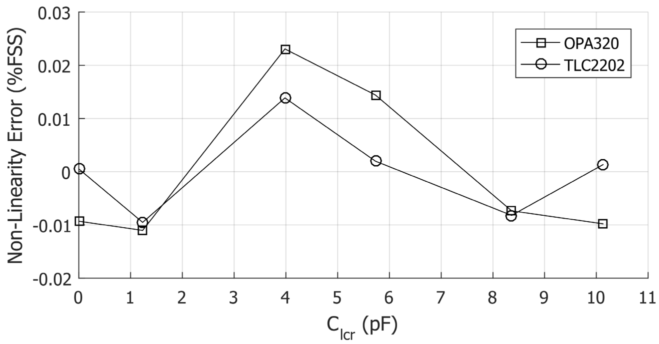

Fig. 9. NLE, relative to FSS. It is computed as the difference between measurements done with the proposed method and the straight lines adjusted in Figs. 5 and 6.

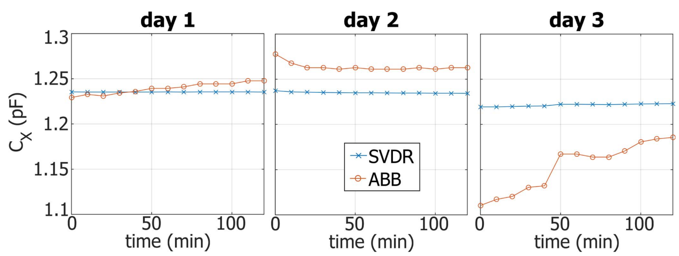

Fig. 10. ABB and SVDR measurements of 1.2-pF capacitor taken on three different days. Note that for the ABB case, C_{IN} was calibrated only once before the first measurement.

measurement of capacitance (regardless of being calibrated or not) and that resulted from the linear fittings depicted in Figs. 5 and 6, relative to the full-scale capacitance (10 pF). This error is depicted in Fig. 9 for the two OAs in the SVDR mode. It can be observed good linearity with a maximum NLE (MNLE) below 0.025% that corresponds to the OPA320 when measuring 3.9 pF; the remaining cases are better but in the same order of magnitude (MNLE $\approx$ 0.015%).

D. Effects of the Cable Length

The response of the circuit in Fig. 4 in the SVDR mode was experimentally evaluated at different cable lengths (5, 10, and 15 m) for both OAs. The capacitances were estimated by applying (5) with the corrected values of the proportionality constant determined before so that any additional gain error could be attributed to the new cable length. For each combination of OA and cable length, a straight line was fitted to the measurements to assess the effects of the cable length on the offset and gain of the input–output characteristic. The MNLE was also computed for each case.

The results are summarized in Table II for four capacitors with a nominal value of 0, 1.2, 5.6, and 10 pF; the LCR measurements (the first column in Table II) were slightly different than those reported in Table I (less than 0.2%) since these corresponded to different measurements carried on in a distinct day. According to Table II, the offset capacitance was very low (between 2 and 3 fF), similar to what was found in Fig. 8, even for a 15-m interconnecting cable and for both OAs. In addition, the input–output characteristic showed an experimental gain error very similar to the error predicted by (11). In terms of linearity, in the worst-case scenario, the MNLE was 0.013 %FSS, which is similar to that reported before in Fig. 9. Therefore, regardless of the cable length, the nonlinearity of the proposed circuit remains very low.

E. Analysis of Time Drifts

The results of the time drift test are represented in Fig. 10. In the ABB mode, the effects of the time drift of C_{IN} on the C_X measurement can be seen from one day to the other (e.g., from day 1 to day 2), and even within the same day (e.g., in day 3). On the contrary, in the SVDR mode, the measurements were clearly much more stable, from one day to the next one, and within the same day. Therefore, the SVDR mode provides a measurement result that is immune to C_{IN} and also to its time drifts.

VI. CONCLUSION

A novel front-end circuit based on a smart driving of the reference node of the OA supply voltage has been proposed and characterized for the measurement of remote grounded capacitive sensors in the 0–10-pF range. The input–output characteristic of the proposed circuit shows, without applying any adjustment and/or calibration, an offset error lower than 3 fF and an NLE lower than 0.025 %FSS. Such a satisfactory performance remains for interconnecting cables up to 15 m. The input–output characteristic does show a gain error that mainly depends on the length of the interconnecting cable, but this can be easily compensated through an OPC. In addition, the proposed circuit does not require any large-volume component, such as a transformer, and hence it is well suited to be integrated.

References

[1] A. Schütze, N. Helwig, and T. Schneider, "Sensors 4.0–smart sensors and measurement technology enable industry 4.0," *J. Sensors Sensor Syst.*, vol. 7, no. 1, pp. 359–371, May 2018.

[2] U. Salmaz, M. A. H. Ahsan, and T. Islam, "High-precision capacitive sensors for intravenous fluid monitoring in hospitals," *IEEE Trans. Instrum. Meas.*, vol. 70, pp. 1–9, 2021.

[3] E. Rando, P. Perez, S. F. Scagliusi, F. J. Medrano, G. Huertas, and A. Yufera, "A plethysmography capacitive sensor for real-time monitoring of volume changes in acute heart failure," *IEEE Trans. Instrum. Meas.*, vol. 70, pp. 1–12, 2021.

[4] O. P. Maurya and P. Sumathi, "A digital interfacing circuit based on sliding DFT bins for capacitive sensors," *IEEE Trans. Instrum. Meas.*, vol. 70, pp. 1–9, 2021.

[5] K. Loizou and E. Koutroulis, "Water level sensing: State of the art review and performance evaluation of a low-cost measurement system," *Measurement*, vol. 89, pp. 204–214, Jul. 2016.

[6] A. Dutta, S. K. Bera, S. Saha, H. Mandal, C. Dey, and S. C. Bera, "Study of a noncontact flow transducer using semicylindrical capacitive sensor," *IEEE Trans. Instrum. Meas.*, vol. 70, pp. 1–10, 2021.

[7] Y. Jung, Q. Duan, and J. Roh, "A 17.4-B delta-sigma capacitance-to-digital converter for one-terminal capacitive sensors," *IEEE Trans. Circuits Syst. II, Exp. Briefs*, vol. 64, no. 10, pp. 1122–1126, Oct. 2017.

[8] F. Reverter, X. Li, and G. C. M. Meijer, "Liquid-level measurement system based on a remote grounded capacitive sensor," *Sens. Actuators A, Phys.*, vol. 138, pp. 1–8, Jul. 2007.

[9] K. C. Baby and B. George, "A simple analog front-end circuit for grounded capacitive sensors with offset capacitance," in *Proc. IEEE Int. Instrum. Meas. Technol. Conf. (IMTC)*, May 2013, pp. 1372–1375.

[10] S. N. Nihtianov and G. C. Meijer, "Application challenges of capacitive sensors with floating targets," in *Proc. IEEE Africon*, Sep. 2011, pp. 1–6. [Online]. Available: http://ieeexplore.ieee.org/document/6072177/

[11] M. Haberman, A. Cassino, and E. Spinelli, "Estimation of stray coupling capacitances in biopotential measurements," *Med. Biol. Eng. Comput.*, vol. 49, no. 9, pp. 1067–1071, Sep. 2011. [Online]. Available: http://www.ncbi.nlm.nih.gov/pubmed/21773804 and http://link.springer.com/10.1007/s11517-011-0811-6

[12] N. Anandan and B. George, "A wide-range capacitive sensor for linear and angular displacement measurement," *IEEE Trans. Ind. Electron.*, vol. 64, no. 7, pp. 5728–5737, Jul. 2017.

[13] Z. Czaja, "A measurement method for capacitive sensors based on a versatile direct sensor-to-microcontroller interface circuit," *Measurement*, vol. 155, Apr. 2020, Art. no. 107547.

[14] F. Reverter, X. Li, and G. C. M. Meijer, "A novel interface circuit for grounded capacitive sensors with feedforward-based active shielding," *Meas. Sci. Technol.*, vol. 19, no. 2, Feb. 2008, Art. no. 025202.

[15] A. A. Bijargah, A. Heidary, P. Torkzadeh, and S. Nihtianov, "An accurate and power-efficient period-modulator-based interface for grounded capacitive sensors," *Int. J. Circuit Theory Appl.*, vol. 47, pp. 1211–1224, May 2019.

[16] R. Joarder and C. S. Anoop, "A linear front-end circuit for offset-affected grounded capacitive sensors," in *Proc. IEEE Region Conf. (TENCON)*, Oct. 2019, pp. 2280–2284.

[17] M. A. Haberman, E. M. Spinelli, and F. Reverter, "High-linearity front-end circuit for remote grounded capacitive sensors," *IEEE Trans. Instrum. Meas.*, vol. 70, pp. 1–8, 2021.

[18] S. M. Huang, A. L. Stott, R. G. Green, and M. S. Beck, "Electronic transducers for industrial measurement of low value capacitances," *J. Phys. E, Sci. Instrum.*, vol. 21, no. 3, p. 242, 1988.

[19] L. Areekath, B. George, and F. Reverter, "A closed-loop capacitance-to-frequency converter for single-element and differential capacitive sensors," *IEEE Trans. Instrum. Meas.*, vol. 69, no. 11, pp. 8773–8782, Nov. 2020.

[20] S. C. Bera, J. K. Ray, and S. Chattopadhyay, "A low-cost noncontact capacitance-type level transducer for a conducting liquid," *IEEE Trans. Instrum. Meas.*, vol. 55, no. 3, pp. 778–786, Jun. 2006.

[21] P. S. Shenil, R. Arjun, and B. George, "Feasibility study of a non-contact AC voltage measurement system," in *Proc. IEEE Int. Instrum. Meas. Technol. Conf. (IMTC)*, May 2015, pp. 399–404.

[22] M. A. Haberman and E. M. Spinelli, "A noncontact voltage measurement system for power-line voltage waveforms," *IEEE Trans. Instrum. Meas.*, vol. 69, no. 6, pp. 2790–2797, Jun. 2020.

[23] J. M. Kootsey and E. A. Johnson, "Buffer amplifier with femtofarad input capacity using operational amplifiers," *IEEE Trans. Biomed. Eng.*, vols. BME–20, no. 5, pp. 389–391, Sep. 1973.

[24] S. Lanyi and M. Pisani, "A high-input-impedance buffer," *IEEE Trans. Circuits Syst. I, Fundam. Theory Appl.*, vol. 49, no. 8, pp. 1209–1211, Aug. 2002.

[25] F. N. Guerrero and E. M. Spinelli, "A two-wired ultra-high input impedance active electrode," *IEEE Trans. Biomed. Circuits Syst.*, vol. 12, no. 2, pp. 437–445, Apr. 2018.

[26] R. Pallás-Areny and J. G. Webster, *Analog Signal Processing*. Hoboken, NJ, USA: Wiley, 1999.

[27] F. N. Guerrero and E. Spinelli, "Surface EMG multichannel measurements using active, dry branched electrodes," in *Proc. 6th Latin Amer. Congr. Biomed. Eng. (CLAIB)*. Paraná, Argentina: Springer, Oct. 2015, pp. 1–4.

[28] E. M. Spinelli and F. Reverter, "On the stability of shield-driver circuits," *IEEE Trans. Instrum. Meas.*, vol. 59, no. 2, pp. 458–462, Feb. 2010.

Marcelo Alejandro Haberman was born in La Plata, Argentina, in 1984. He received the Engineering degree in electronics and the Ph.D. degree from La Plata National University (UNLP), La Plata, in 2008 and 2016, respectively.

Since 2008, he has been with the Institute for Research in Electronics, Signal Processing, and Control (LEICI), Faculty of Engineering, UNLP, and CONICET. His current research interests include electronic instrumentation and mixed (analog/digital) signal processing for noninvasive measurements of voltage and impedance.

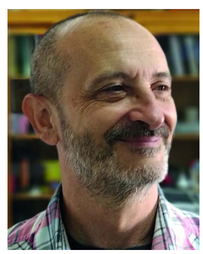

Enrique Mario Spinelli was born in Balcarce, Argentina, in 1964. He received the Engineering degree in electronics and the Ph.D. degree from La Plata National University (UNLP), La Plata, Argentina, in 1989 and 2006, respectively.

Since 1990, he has been with the Institute for Research in Electronics, Signal Processing, and Control (LEICI), Faculty of Engineering, UNLP, and CONICET. His current research interests include analog signal processing and human–machine interfaces.

Ferran Reverter was born in Llagostera, Spain, in 1976. He received the B.Sc. degree in industrial electronic engineering from the University of Girona, Girona, Spain, in 1998, the M.Sc. degree in electronic engineering from the University of Barcelona, Barcelona, Spain, in 2001, and the Ph.D. degree in electronic engineering from the Universitat Politècnica de Catalunya (UPC), Barcelona, in 2004.

Since 2001, he has been with UPC, where he is currently an Associate Professor in analog electronics, digital systems, and sensors. He was a Visiting Post-Doctoral Researcher with the Delft University of Technology, Delft, The Netherlands, from 2005 to 2007, and with the Imperial College London, London, U.K., in 2012. Since 2018, he has also been with the Open University of Catalonia (UOC), Barcelona, where he is also a Course Instructor in electronic instrumentation. His current research interests include interface electronics for smart sensors, power-processing circuits for autonomous sensors, and MOSFET thermal sensors for IC testing.

Dr. Reverter was awarded as an "Outstanding Reviewer" from the IEEE Instrumentation and Measurement Society three times in 2014, 2018, and 2019. He was an Associate Editor of the IEEE Sensors Journal from 2015 to 2022 and IEEE Transactions on Instrumentation and Measurement from 2018 to 2022.